Experimental and theoretical insights into binary Zn-SBA-15/KI catalysts for the selective coupling of CO_2 and epoxides into cyclic carbonates under mild conditions

Mengshuai Liu,‡[a] Kunqi Gao,‡[a] Lin Liang,[c] Jianmin Sun,*[b,a] Li Sheng,*[a] and Masahiko Arai*[d]

[a] *MIIT Key Laboratory of Critical Materials Technology for New Energy Conversion and Storage, School of Chemistry and Chemical Engineering, Harbin Institute of Technology, Harbin 150080, PR China*

[b] *State Key Laboratory of Urban Water Resource and Environment, Harbin Institute of Technology, Harbin 150080, PR China*

[c] *School of Life Science and Technology, Harbin Institute of Technology, Harbin 150080, PR China*

[d] *Division of Applied Chemistry, Faculty of Engineering, Hokkaido University, Sapporo 060-8628, Japan*

Abstract: The combination of metal modified SBA-15 catalyst with potassium iodide was developed as heterogeneous dual catalysts for chemical fixation of CO_2 to cyclic carbonates. It was observed that the binary Zn-SBA-15/KI catalysts were the most efficient among various metal modified SBA-15/KI catalysts and showed excellent synergetic effect in promoting the reaction under mild conditions. Moreover, the effects of reaction parameters on cycloaddition of CO_2 with propylene oxide (PO) to propylene carbonate (PC) were optimized. Under the optimal conditions determined, Zn-SBA-15/KI catalytic system was also versatile to CO_2 cycloaddition with other epoxides. Additionally, the mechanistic details for the fixation of CO_2 into cyclic carbonate catalyzed by SBA-15/KI and Zn-SBA-15/KI were also contrastively elucidated using the density functional theory (DFT) method. The DFT results suggested that zinc-modified and unmodified catalysts showed different coupling modes of CO_2, and the

‡ These authors contributed equally to this work.

* Corresponding authors. Tel.: +86 451 86403715; fax: +86 451 86403715.

E-mail address: sunjm@hit.edu.cn (J.M. Sun), shengli@hit.edu.cn (L. Sheng), marai@eng.hokudai.ac.jp (M. Arai).

ring-opening reaction was the rate-determining step in the SBA-15/KI catalyzed cycloaddition reaction, but the zinc-modified SBA-15/KI catalysts could enhance the CO_2 cycloaddition as the formation of a stable complex which was beneficial to CO_2 trapping. As a result, the ring-closing reaction became the rate-determining step in the Zn-SBA-15/KI catalyzed cycloaddition reaction, which were promising results to guide the catalyst design for CO_2 conversion.

Keywords: Carbon dioxide; Cyclic carbonate; Potassium iodide; Zn-SBA-15; DFT calculation

Introduction

Carbon dioxide, one of the undesired greenhouse effect gases, is an abundant, inexpensive, and non-toxic renewable C1 resource and so the development of efficient catalytic process for CO_2 transformation into value-added products is a challenging and practically important task.[1] One of the most promising strategies is the catalytic synthesis of cyclic carbonates *via* 100% atom-economical coupling reactions of CO_2 and epoxides (Scheme 1),[2] since it represents a much greener alternative to the traditional phosgene process, and the cyclic carbonates have found several potential applications ranging from polar aprotic solvents to intermediates in the manufacture of fine chemicals.[3]

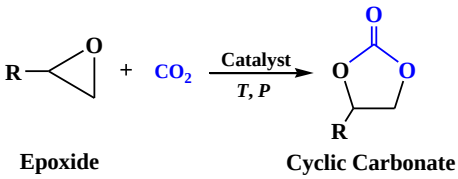

Scheme 1 Cycloaddition of CO_2 to epoxides.

In the past few decades, various homogeneous and heterogeneous catalysts have been developed for the cycloaddition of CO_2 to epoxides, including metal-oxides,[4] *N*-heterocyclic carbenes,[5] metal-salen complexes,[6] ammonium or phosphonium salts,[7] metal-organic frameworks,[8] alkali metal salts,[9] and ionic liquids.[10] It is worth mentioning that the alkali metal salt of KI is one of potential catalyst components, which is cheap, nontoxic, abundant, and easily recyclable, although it is much less active by itself. The concurrent use of KI and other components, such as cellulose,[11] C_{60} fullerenol,[12] amino acid,[13] lignin[14] and Fe_3O_4@$Fe(OH)_3$,[15] give enhanced catalytic activity for the coupling reaction of CO_2 and epoxides. However, the activity observed so far is not satisfactory and high CO_2 pressure and temperature are still necessary.[16] It is suggested that surface hydroxy groups and/or Zn sites on solid catalysts act as Lewis acid sites, which may activate the epoxide then facilitate its ring opening.[17]

After considering those previous results, the present work has been undertaken to

design active catalysts for the cycloaddition of CO_2 to epoxides through synergistic effects of hydroxyl groups and Zn sites on SBA-15 and a co-catalyst of KI. The authors prepared several metals (Zn, Fe, Ni, Co) modified SBA-15 samples cooperating with KI as binary catalysts and applied these catalysts for the selective coupling of CO_2 and epoxides into cyclic carbonates under mild conditions. The combination of Zn-BA-15 and KI was observed to be the most effective, and then the preparation and reaction conditions were optimized for the catalyst system. The designed binary catalyst system (Zn-SBA-15/KI) has been found to give satisfactory results involving epoxide conversion and cyclic carbonate selectivity under milder conditions (80 ºC, 1 MPa CO_2) compared to the newly reported heterogeneous catalytic systems, such as ceria and lanthanum doped zirconia (170 ºC, 7.0 MPa),[18] g-C_3N_4/SBA-15 (150 ºC, 3.5 MPa),[19] MCM-41 immobilized imidazole bromide (140 ºC, 4.0 MPa),[20] amino/ hydroxyl-rich graphitic carbon nitride (130 ºC, 3.5 MPa)[21] and zinc-coordinated conjugated microporous polymer (120 ºC, 3.0 MPa)[22] (detailed conditions and comparison will be given later in Table 4). In addition, the recyclability of our catalyst system was examined for a selected coupling reaction of CO_2 and propylene oxide (PO). Possible reaction mechanisms and catalytic actions over Zn-SBA-15/KI and SBA-15/KI were also contrastively elucidated via a model calculation based on the density functional theory (DFT) method.

Results and discussion

Structural features of SBA-15 based catalysts

Fig. 1 gives FTIR spectra of several metal species modified SBA-15 samples. Our attention was paid to an absorption band at 960 cm^{-1} attributable to asymmetric stretching of Si–O of surface Si–OH structure.[23] For unmodified SBA-15, an absorption band was observed at 960 cm^{-1}, indicating the presence of surface silanol groups. This relative intensity of the absorption band was gradually weakened on the modification of Zn, Fe, Ni and Co species. And it was little detected for the Zn-SBA-15 sample with increasing amounts of Zn species (Zn/Si = 0.15, 0.18), suggesting that Zn species were

loaded onto the surface of SBA-15 at expense of its silanol groups.[24]

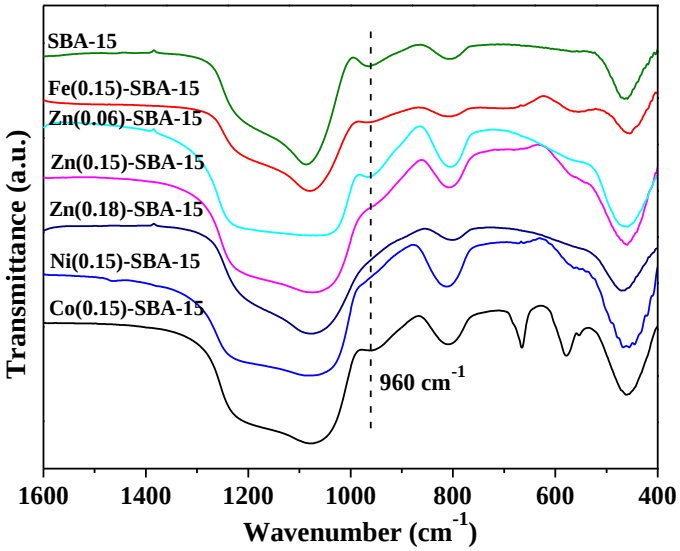

Fig. 1 FT-IR spectra of SBA-15 modified with different metal species.

XRD patterns for SBA-15 and M-SBA-15 samples are shown in Fig. 2. From the small-angle XRD patterns (Fig. 2A), all M-SBA-15 samples showed good orderings of 2D-hexagonal P6mm structure indexed to (100), (110) and (200) reflections,[25] indicating their mesoporous structure. And the intensities of (100) reflection increased in some cases compared with pristine SBA-15, due to the formation of Si-O-M monolayer or MO_x layer on the surface of SBA-15.[25b] Wide-angle XRD patters of Fig. 2B indicated the presence of crystalline Fe_2O_3 phase (hematite) (2θ = 34.7°, 35.6°, 54.2°, 63.0°)[26] for Fe(0.15)-SBA-15 sample and Co_3O_4 spinel structure (2θ = 19.0°, 31.3°, 36.9°, 44.9°, 59.4°)[27] for Co(0.15)-SBA-15 catalyst sample. For Ni(0.15)-SBA-15 sample as well, NiO phase (2θ = 37.2°, 43.3°, 62.9°) was detected.[28] In contrast to these metal-modified SBA-15 samples, such metal oxide phase was not detected for Zn(0.15)-SBA-15 sample although the metal loading was the same as in those samples (M/Si = 0.15). Hence, the metal species added were highly dispersed on the surface of SBA-15 for Zn but not for the other metals (Fe, Co, Ni).

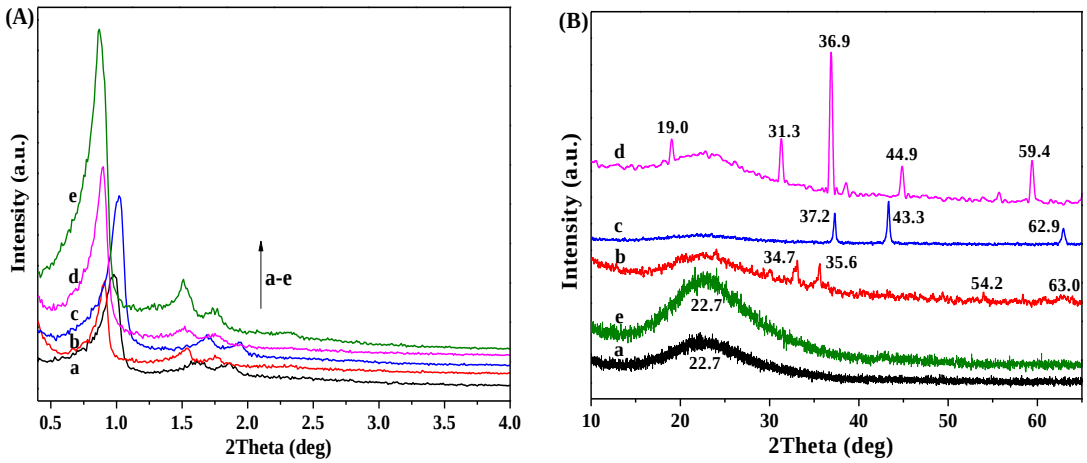

Fig. 2 (A) Small-angle and (B) wide-angle XRD patterns of SBA-15 samples modified with different metal species. (a) SBA-15, (b) Fe(0.15)-SBA-15, (c) Ni(0.15)-SBA-15, (d) Co(0.15)-SBA-15, (e) Zn(0.15)-SBA-15.

For Zn(0.15)-SBA-15 sample, the pore structure was examined by N_2 adsorption and TEM. As shown in Fig. 3, its N_2 adsorption-desorption isotherm was of type IV curve with H1 hysteresis loop, which evidenced its ordered mesoporous structure. The BET surface area, pore diameter, and pore volume were determined to be 517 m^2 g^{-1}, 7.5-11.0 nm, and 0.81 cm^3 g^{-1}, respectively. Compared with pristine SBA-15,[29] it was observed that both the surface area and pore volume of zinc modified SBA-15 decreased, indicating zinc species were successfully dispersed on the surface of SBA-15. A TEM image (Fig. 3C) clearly showed the long-range channel ordering. It should be mentioned again that the Zn additive was highly dispersed on the surface of SBA-15 and its mesoporous structure remained unchanged for a sample containing a larger amount of Zn (Zn/Si = 0.15). These structural features would be beneficial to the target coupling reaction of CO_2 and epoxides.

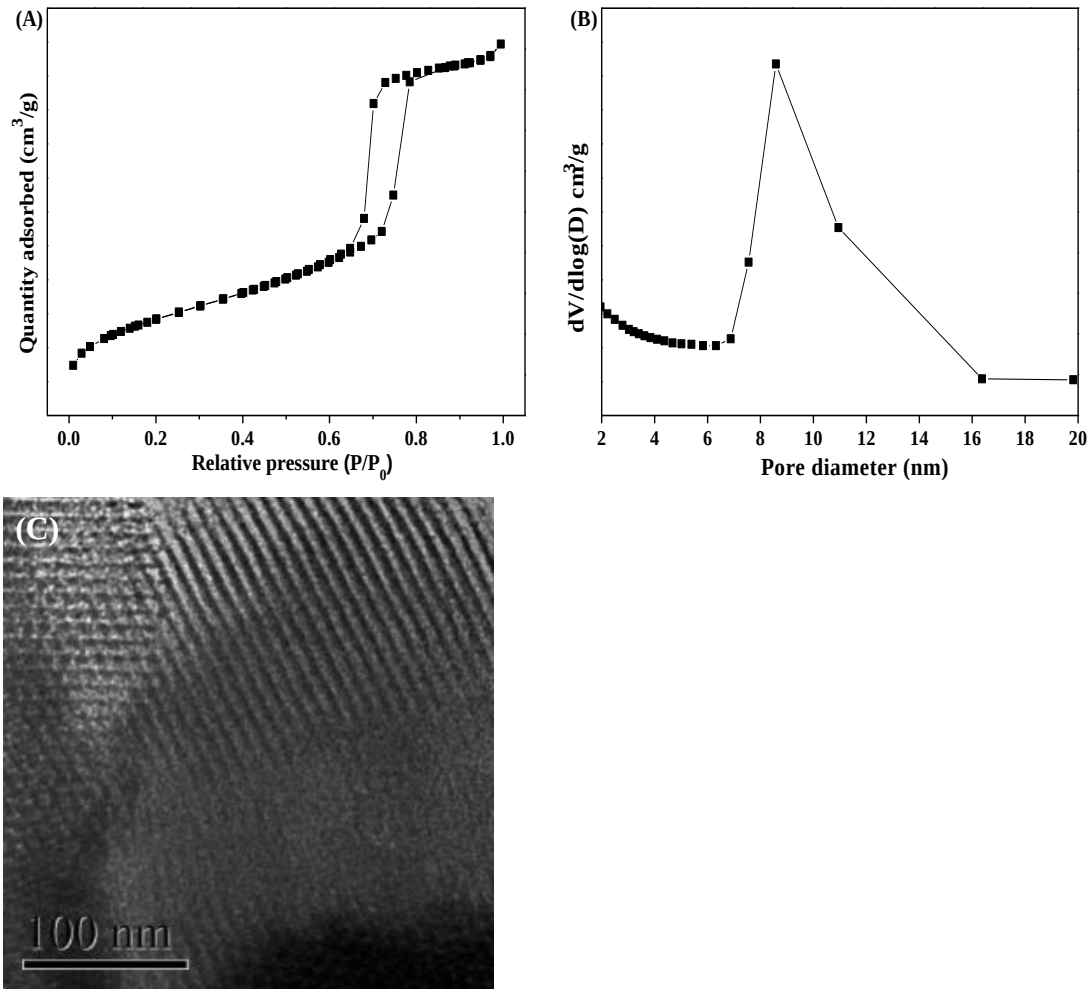

Fig. 3 (A) N_2 adsorption/desorption isotherm, (B) pore size distributions and (C) TEM image of Zn(0.15)-SBA-15 sample.

Catalytic performance of SBA-15 based catalysts

(a) Comparison among SBA-15 samples modified with different metal species

The catalytic activities of various metal modified SBA-15 samples with KI co-catalyst were tested towards the model reaction of CO_2 cycloaddition to PO, and the results are summarized in Table 1. No product was detected to form when either SBA-15 or KI was used (entries 1, 2) at 80 ^oC and 1.0 MPa for 9.0 h, and only 4% PC yield was obtained for KI at higher temperature of 120 ^oC for 3.0 h (entry 3). When both SBA-15 and KI components were used, PC was selectively formed in a yield of 53% under the conditions used (entry 4), indicating synergistic effects of –OH on surface of SBA-15 and KI. Although a Zn-modified SBA-15 catalyst alone was inactive (entry 5), a high PC yield of 96% was achieved with the same catalyst in the presence of KI (entry

6). The addition of Ni species did not affect the activity of SBA-15 catalyst (entry 7) while Fe(0.15)- or Co(0.15)-SBA-15 catalysts yielded a better PC yield of about 80% (entries 8, 9), as compared to that obtained with the unmodified SBA-15 sample (entry 4). With those unmodified and metal modified SBA-15 samples, PC was selectively produced.

For the most active Zn-SBA-15 catalyst, the influence of Zn loading was examined. When the Zn loading was small (Zn/Si = 0.05), the PC yield obtained was comparable to that with unmodified SBA-15 sample (entries 4, 10). With an increase in Zn loading from Zn/Si = 0.05 to 0.15, the catalytic activity was significantly improved (entries 6, 10, 11). While further increasing Zn/Si molar ratio up to 0.20, the activity decreased with PC yield of 88% (entry 12). The decrease of PC yield might be ascribed to the fact that the excess zinc species cover on the top of Si-O-Zn layer and convert to the smooth ZnO layer on the surface of SBA-15,[25b] then decrease both the surface area and pore volume of zinc modified SBA-15. Thus, there existed an optimal Zn loading, which was about Zn/Si = 0.15. As confirmed from FTIR of Zn-SBA-15 (Fig. 1), at Zn/Si molar ratio of 0.15, the band at 960 cm^{-1} was almost invisible, demonstrating that the loaded Zn species consumed all the silanol groups on SBA-15.[29] Additionally, a reaction run was made at a higher temperature of 120 ºC, at which a high PC yield of 98% was achieved in a shorter reaction time of 2 h (entry 13).

Table 1 Catalyst screening for the cycloaddition of CO_2 to PO[a]

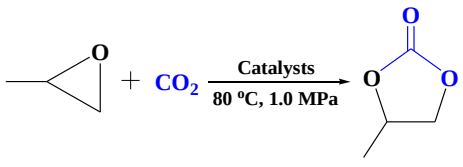

PO **PC**

Entry	Catalyst	Co-catalyst	Reaction results[b]	
			Y_{PC} (%)	S_{PC} (%)
1	SBA-15	—	trace	—
2	—	KI	trace	—
3[c]	—	KI	4	≥98

4	SBA-15	KI	53	≥ 99
5	Zn(0.15)-SBA-15	—	trace	≥ 99
6	Zn(0.15)-SBA-15	KI	96	≥ 99
7	Ni(0.15)-SBA-15	KI	54	≥ 99
8	Fe(0.15)-SBA-15	KI	79	≥ 99
9	Co(0.15)-SBA-15	KI	81	≥ 99
10	Zn(0.05)-SBA-15	KI	59	≥ 99
11	Zn(0.10)-SBA-15	KI	85	≥ 99
12	Zn(0.20)-SBA-15	KI	88	≥ 99
13[d]	Zn(0.15)-SBA-15	KI	98	≥ 99

[a] Reaction conditions: PO 2.0 g (34.5 mmol), catalyst 0.05 g, KI 0.3mmol, T = 80 °C, P (CO_2) = 1.0 MPa, t = 9.0 h. [b] Y_{PC}: PC yield; S_{PC}: PC selectivity; all based on GC analysis. [c] T = 120 °C, P (CO_2) = 1.0 MPa, t = 3.0 h. [d] T = 120 °C, t = 2.0 h.

(b) Effects of catalyst loadings

Next, the influence of catalyst (Zn-SBA-15, KI) loadings on the PC synthesis was investigated over the above-mentioned most active Zn(0.15)-SBA-15 catalyst with a co-catalyst of KI. Table 2 shows that the amounts of these two catalytic components varied the PC yield significantly but not the PC selectivity. PC was exclusively produced under any conditions used. With a fixed KI amount of 0.30 mmol, the PC yield was dramatically increased from 29% to 96% by increasing the amount of Zn(0.15)-SBA-15 from 0.01 g to 0.05 g (entries 1–3). However, no enhancement in the PC yield was observed when it was further increased to 0.06 g (entry 4). On the other hand, at a fixed amount of 0.05 g Zn(0.15)-SBA-15, the PC yield was increased with the amount of KI in the range of 0.06 - 0.30 mmol (entries 3, 5, 6) but the PC yield with 0.42 mmol KI was comparable to that with 0.30 mmol (entries 3, 7). Thus, those results indicate that an equivalent-mass mixture of Zn(0.15)-SBA-15 and KI catalyst components (1:3 molar ratio of zinc species to KI) was optimal for the synthesis of PC via coupling of CO_2 and PO.

Table 2 Effect of catalyst loadings on the PC synthesis over Zn(0.15)-SBA-15/KI system [a]

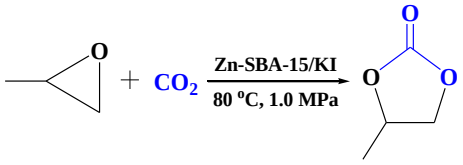

PO **PC**

Entry	Weight of catalytic components		Reaction results[b]	
	Zn(0.15)-SBA-15 (g)[c]	KI (mmol)	Y_{PC} (%)	S_{PC} (%)
1	0.01	0.30	29	≥ 99
2	0.03	0.30	80	≥ 99
3	0.05	0.30	96	≥ 99
4	0.06	0.30	97	≥ 99
5	0.05	0.06	12	≥ 99
6	0.05	0.18	67	≥ 99
7	0.05	0.42	99	≥ 99

[a] Reaction conditions: PO 2.0 g (34.5 mmol), T = 80 °C, P (CO_2) = 1.0 MPa, t = 9.0 h. [b] Y_{PC}: PC yield; S_{PC}: PC selectivity; all based on GC analysis. [c] Zinc concentration analyzed by ICP-OES was 1.8 mmol/g.

(c) Effects of reaction parameters

Using the most active Zn(0.15)-SBA-15/KI catalysts with an optimized loadings, the PC synthesis was studied at different temperature, CO_2 pressure and time to optimize these reaction variables. Table 3 shows a significant impact of temperature on the PC yield (entries 1–5). A higher temperature was better for a higher PC yield in the range of 50–80 ºC, at which the selectivity to the desired product of PC was almost perfect. Further raising temperature to 90 ºC was insignificant, comparable high PC yields of 96% and 98% being obtained at 80 ºC and 90 ºC.

A PC yield of 81% was obtained at a CO_2 pressure of 0.5 MPa (entry 6) and it was enhanced to 96% at a higher pressure of 1.0 MPa (entry 4). And no significant positive effect was observed by further raising the pressure up to 2.0 MPa (entries 7, 8). Because

when CO_2 pressure is raised, CO_2 molecules as reactant are more likely to dissolve into the substrate (PO) phase, which will cause positive impact on the coupling of PO and CO_2. However, when further raising the CO_2 pressure up to 6.0-7.0 MPa, an obvious negative influence appeared (entries 9, 10), which could be explained that the dissolved adjacent supercritical CO_2 molecules act as a diluent, and the dilution of the epoxide and catalysts likely contributed to the drop in reaction rate and gave a negative impact.[30] The positive impact should be more significant at low CO_2 pressure while the negative impact at high pressure. Under the conditions used, a low CO_2 pressure of 1.0 MPa is sufficient for the synthesis of PC.

Furthermore, the change of PC yield with time was examined under the optimized reaction conditions (entries 4, 11–14). The coupling of CO_2 and PO went smoothly with time and the reaction was almost completed within 9.0 h with the perfect selectivity to PC (entry 4), and further prolonging the reaction time resulted in uncompetitive product yield (entry 14).

Table 3 Effects of reaction parameters on the PC synthesis over Zn(0.15)-SBA-15/KI catalysts[a]

Entry	Temperature (°C)	Pressure (MPa)	Time (h)	Reaction results[b]	
				Y_{PC} (%)	S_{PC} (%)
1	50	1.0	9.0	52	≥ 99
2	60	1.0	9.0	72	≥ 99
3	70	1.0	9.0	86	≥ 99
4	80	1.0	9.0	96	≥ 99
5	90	1.0	9.0	98	≥ 99
6	80	0.5	9.0	81	≥ 99
7	80	1.5	9.0	97	≥ 99
8	80	2.0	9.0	98	≥ 99
9	80	6.0	9.0	32	≥ 99
10	80	7.0	9.0	19	≥ 99
11	80	1.0	2.0	35	≥ 99

12	80	1.0	4.5	76	≥ 99
13	80	1.0	6.0	83	≥ 99
14	80	1.0	10.0	98	≥ 99

[a] Reaction conditions: PO 2.0 g (34.5 mmol), Zn(0.15)-SBA-15 0.05 g, KI 0.3 mmol. [b] Y_{PC}: PC yield; S_{PC}: PC selectivity; all based on GC analysis.

The above-mentioned results demonstrate that the synthesis of PC via coupling of PO and CO_2 can be achieved in the coexistence of Zn-modified SBA-15 and KI under mild temperature and CO_2 pressure (80 ºC, 1.0 MPa). Table 4 compares the results of PC synthesis using various heterogeneous catalysts reported in the literature. The outstanding catalytic performance of our catalyst system involving Zn-modified SBA-15 with high surface area, long-range mesoscopic ordering of the pores and superior stability cooperated with KI under mild conditions is of great significance for practical synthesis of PC and other cyclic carbonates (as described later).

Table 4 Comparison among various catalysts in the performance for the coupling of PO and CO_2

Catalyst	Temp./ ºC	Pressure/ MPa	Cat. loading/ wt%	Time/ h	Yield/ %	Ref.
cellulose/KI	110	2.0	17.2	2.5	99.0	[11]
C_{60} fullerenol/KI[a]	120	2.0	2.9	7.0	91.0	[12]
amino acid/KI[b]	120	1.0	1.0	3.0	98.0	[13]
Lignin/KI	140	2.0	9.2	12.0	93.0	[14]
Fe_3O_4@$Fe(OH)_3$/KI	125	2.0	6.3	1.0	90.8	[15]
β-cyclodextrin/KI	120	6.0	15.8	4.0	98.0	[31]
Ce-La-Zr-O[c]	170	7.0	10.0	20.0	66.0	[18]
MIL-68(In)NH_2[d]	150	0.8	—	8.0	74.0	[32]
Zn-doped g-C_3N_4/SBA-15	150	3.5	4.0	1.5	97.1	[19]
MCM-41-Imi/Br[e]	140	4.0	8.3	6.0	81.5	[20]

g-C_3N_4-S-80[f]	130	3.5	0.9	2.0	98.6	[21]
Zn-CMPs/TBAB[g]	120	3.0	2.0[h]	1.0	94.1	[22]
n-ButBr/mp-C_3N_4[i]	140	2.5	2.4	6.0	87.7	[33]
DMF/Zn-SBA-15	160	2.0	55.0	6.0	92.3	[29]
u-g-C_3N_4-480[j]	130	2.0	8.0	8.0	67.2	[34]
Gea-MOF-1/TBAB	120	2.0	—	6.0	88.0	[35]
Zn-SBA-15/KI	80	1.0	5.0	9.0	96.0	This work

[a] Towards the cycloaddition of CO_2 to styrene oxide. [b] The amino acid means histidine catalyst. [c] Ceria and lanthana doped zirconia. [d] DMF as solvent. [e] Acetonitrile as solvent. [f] Synthesized by protonation of pristine g-C_3N_4 with H_2SO_4 (60%) at 80 °C for 2 h. [g] Zn-CMPs: zinc-coordinated conjugated microporous polymers. [h] mole fraction. [i] Mesoporous carbon nitride grafted with *n*-bromobutane. [j] Prepared using urea as a starting material without addition of any template.

(d) Reusability of Zn(0.15)-SBA-15/KI binary catalysts

Fig. 4 shows the results of repeated reactions of the PC synthesis. When the catalysts mixture were separated by centrifuge after a run and used for the next run, a moderate loss of PC yield was observed even though the perfect PC selectivity remained unchanged. This should be due to a loss of a component of KI because it is soluble into the organic PO (and PC) phase to some extent. The heterogeneous Zn-SBA-15 catalyst can be completely recycled with high stability and catalytic activity. Theoretically speaking, the soluble part of KI co-catalyst can also be recycled by vacuum distillation of the formed cyclic carbonate, and integrated into the recycled system to participate in the next round, but not make ends meet. To understand the recyclability and stability of the Zn-SBA-15/KI catalytic system, an amount of fresh KI equivalent to the soluble amount (about 20% of the initial amount of KI) was added to control the preset total amount of Zn-SBA-15 and KI to 0.1 g, the same high PC yield as observed in the first run appeared again. No additional Zn-SBA-15 was needed, which suggested no leaching of zinc species.

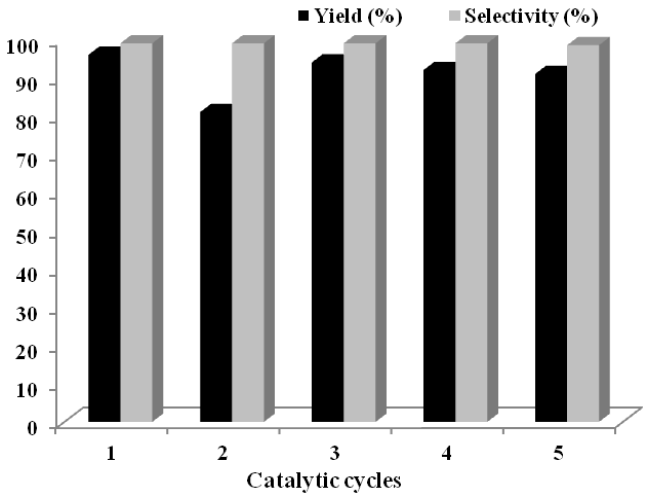

Fig. 4 Recyclability of the catalysts. Conditions: PO 2.0 g (34.5 mmol), Zn(0.15)-SBA-15 0.05 g, KI 0.3 mmol, T = 80 °C, P (CO_2) = 1.0 MPa, t = 9.0 h.

(e) Cycloaddition of CO_2 to various epoxides

The versatility of our binary Zn-SBA-15/KI catalytic system was further studied by applying for the coupling reaction of CO_2 with different epoxides. Table 5 shows that four terminal epoxides were successfully transformed to their corresponding cyclic carbonate products over Zn(0.15)-SBA-15/KI under the optimum conditions (entries 1–4). The conversion rate of styrene oxide that having a large phenyl ring was smaller, with a product yield of 84% (entry 4), due to its steric hindrance compared to the other ones (entry 1–3). For a disubstituted epoxide of cyclohexene oxide, a low product yield of 36% was obtained even at a higher temperature of 120 °C and a longer reaction time of 12 h although the selectivity to the cyclic carbonate was perfect (entry 5) similar to the other epoxides.

Table 5 Coupling reactions of CO_2 with various epoxides over Zn(0.15)-SBA-15/KI catalysts[a]

Entry	Epoxide	Product	T (°C)	t (h)	Reaction results[b]	
					Y_{PC} (%)	S_{PC} (%)
1		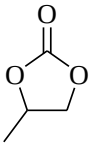	80	9.0	96	99

2	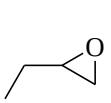	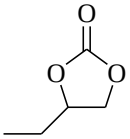	80	9.0	92	99
3	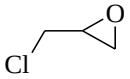	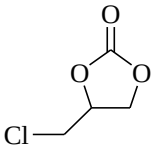	80	9.0	99	99
4	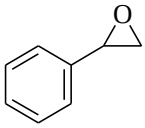	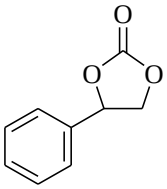	80	9.0	84	99
5[c]	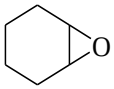	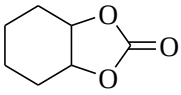	120	12.0	36	98

[a] Reaction conditions: epoxide 34.5 mmol, Zn(0.15)-SBA-15 0.05 g, KI 0.3 mmol, *P* (CO_2) = 1.0 MPa. [b] Y_{PC}.: product yield; S_{PC}: product selectivity; all based on GC analysis. [c] *P* = 2.0 MPa.

Possible reaction mechanisms

The selective synthesis of cyclic carbonates via coupling of epoxides and CO_2 can be achieved with Zn-SBA-15 catalyst in the presence of co-catalyst of KI, as above-mentioned. The optimum molar ratio of Zn against Si was 0.15, at which surface hydroxyl groups on SBA-15 almost disappeared (Fig. 1). The relative amounts of Zn-SBA-15 and KI were also important and their equivalent-mass (1:3 molar ratio of zinc species to KI) mixture was optimum. As the O atom of Zn-SBA-15 (or SBA-15) catalyst undergo electrostatic interaction with the K^+ cation,[36] KI species exist on the surface of Zn-SBA-15 in the reaction system. According to the present results and the previous ones reported in the literature,[28,37] we proposed plausible reaction mechanism for the CO_2 cycloaddition to epoxide over Zn(0.15)-SBA-15/KI catalysts (Scheme 2). The cycloaddition reaction is initiated by binding the oxygen atom of epoxide with the Lewis acidic zinc site of Zn(0.15)-SBA-15 through the formation of zinc-epoxide complex to activate the epoxy ring (Step 1). And simultaneously, activated epoxide molecule opens the epoxy ring *via* S_N1 mechanism, and KI stabilizes the ring-opened intermediate Int_{B-1}(Step 2). Subsequently, CO_2 molecule is coupled with the alkoxide.

Meanwhile, the O atom of CO_2 coordinates with Zn (Step 3), which results in a stable alkyl carbonate intermediate Int_{B-3} (Step 4). Finally, with an S_N2-type replacement reaction, the cyclic carbonates are produced and the catalysts are regenerated (Step 5). Hence, the activation of Zn together with the stabilization ability of KI smoothly promoted the cycloaddition reaction under mild conditions.

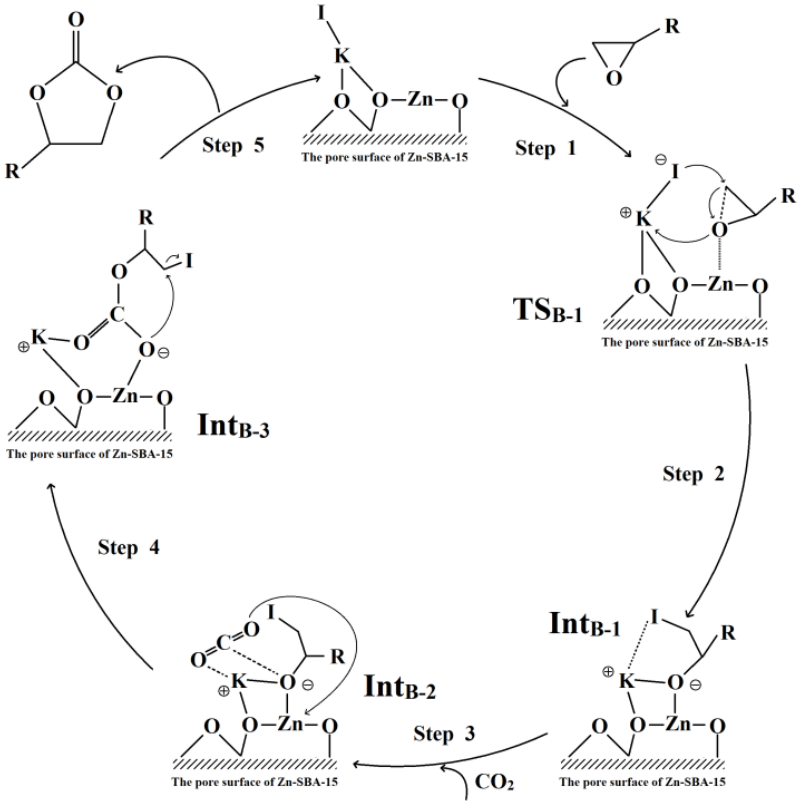

Scheme 2 Proposed mechanism for Zn-SBA-15/KI catalyzed cycloaddition reaction of CO_2 and epoxide.

As comparison, the CO_2 cycloaddition to epoxide over SBA-15/KI catalysts is shown in Scheme 3. The cycloaddition reaction is initiated by binding the oxygen atom of epoxide with the hydrogen bond donor -OH of SBA-15 through forming hydrogen bonds (Step 1). And simultaneously, I^- anion attacks the less sterically hindered β-carbon atom of epoxide, facilitating the ring-opening of epoxide *via* S_N2 mechanism (Step 2). Subsequently, CO_2 molecule is adsorbed with the alkoxide (Step 3). Through a transition state with low energy barrier, an unstable alkyl carbonate intermediate Int_{A-}

$_3$ is obtained (Step 4). Finally, with an S_N2-type replacement reaction, the cyclic carbonates are produced and the catalysts are regenerated (Step 5). The epoxide activation then subsequent nucleophilic attack of I^- anion determined the process of the cycloaddition reaction.

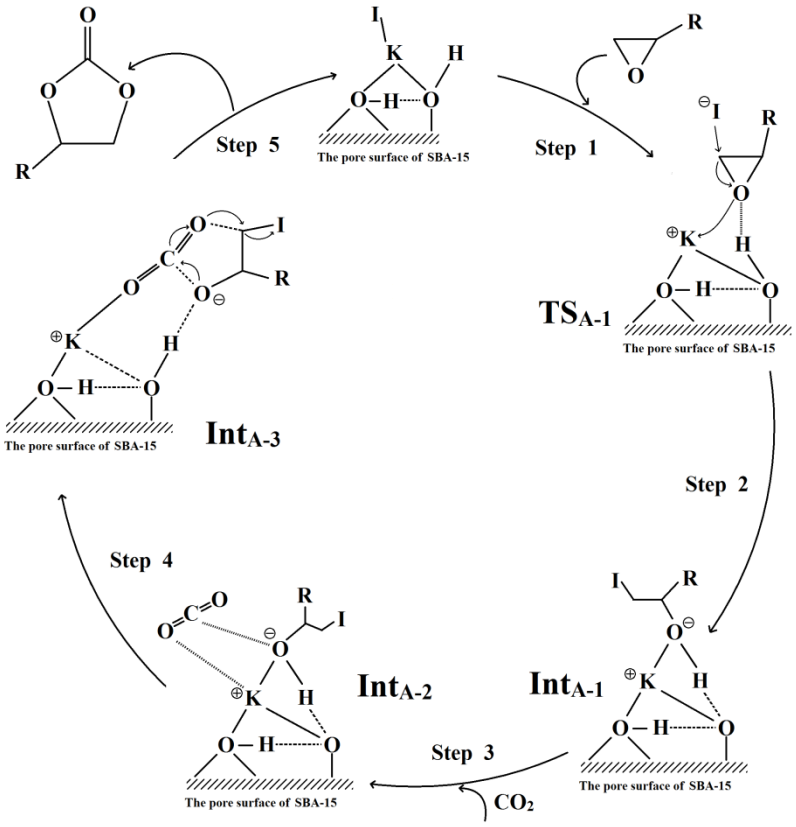

Scheme 3 Proposed mechanism for SBA-15/KI catalyzed cycloaddition reaction of CO_2 and epoxide.

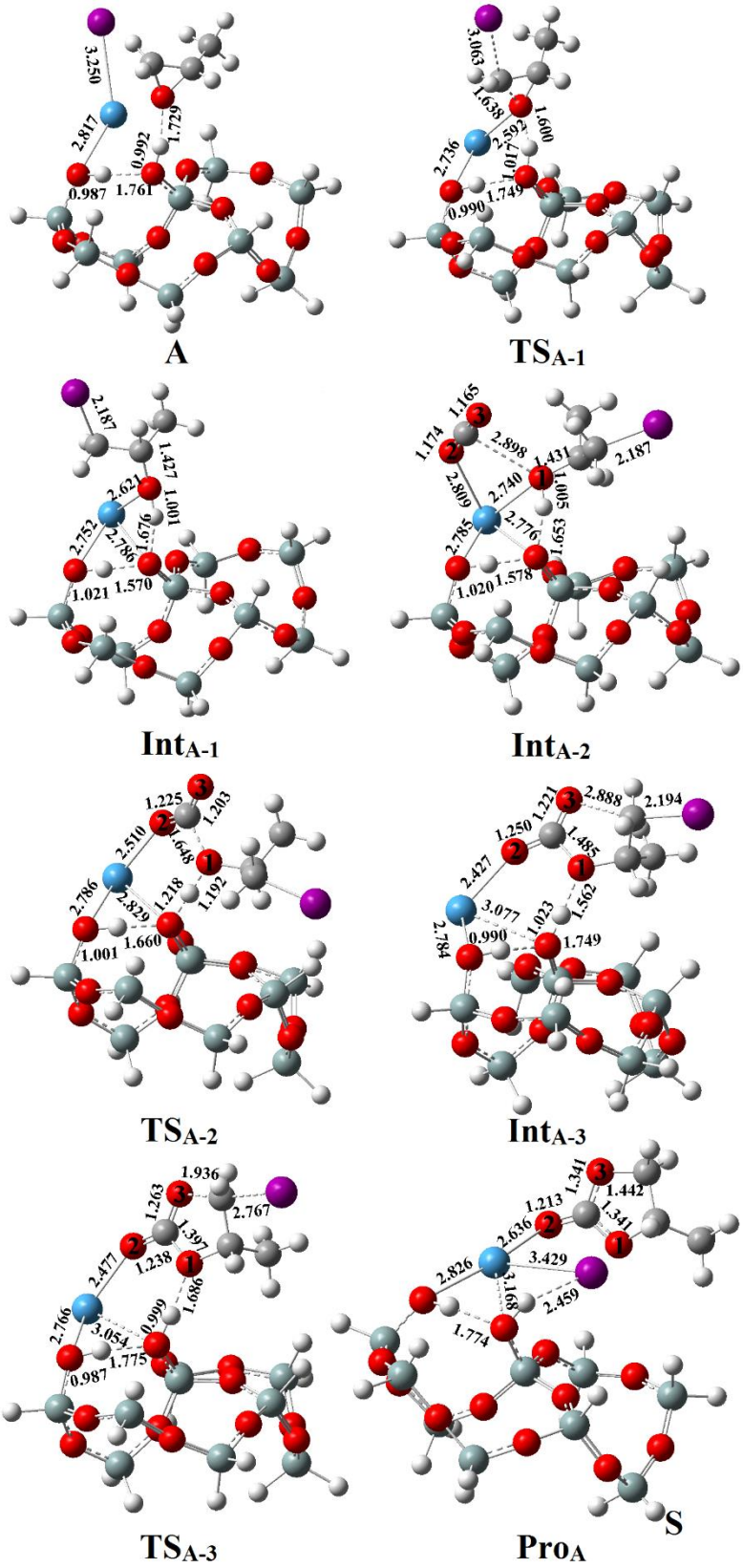

Fig. 5 The B3LYP/6-31G(d) optimized geometries of reactants, intermediates, transition states and products in Reaction A catalyzed by SBA-15/KI . Si – cyan, O – red, H – white, K – blue, I – purple.

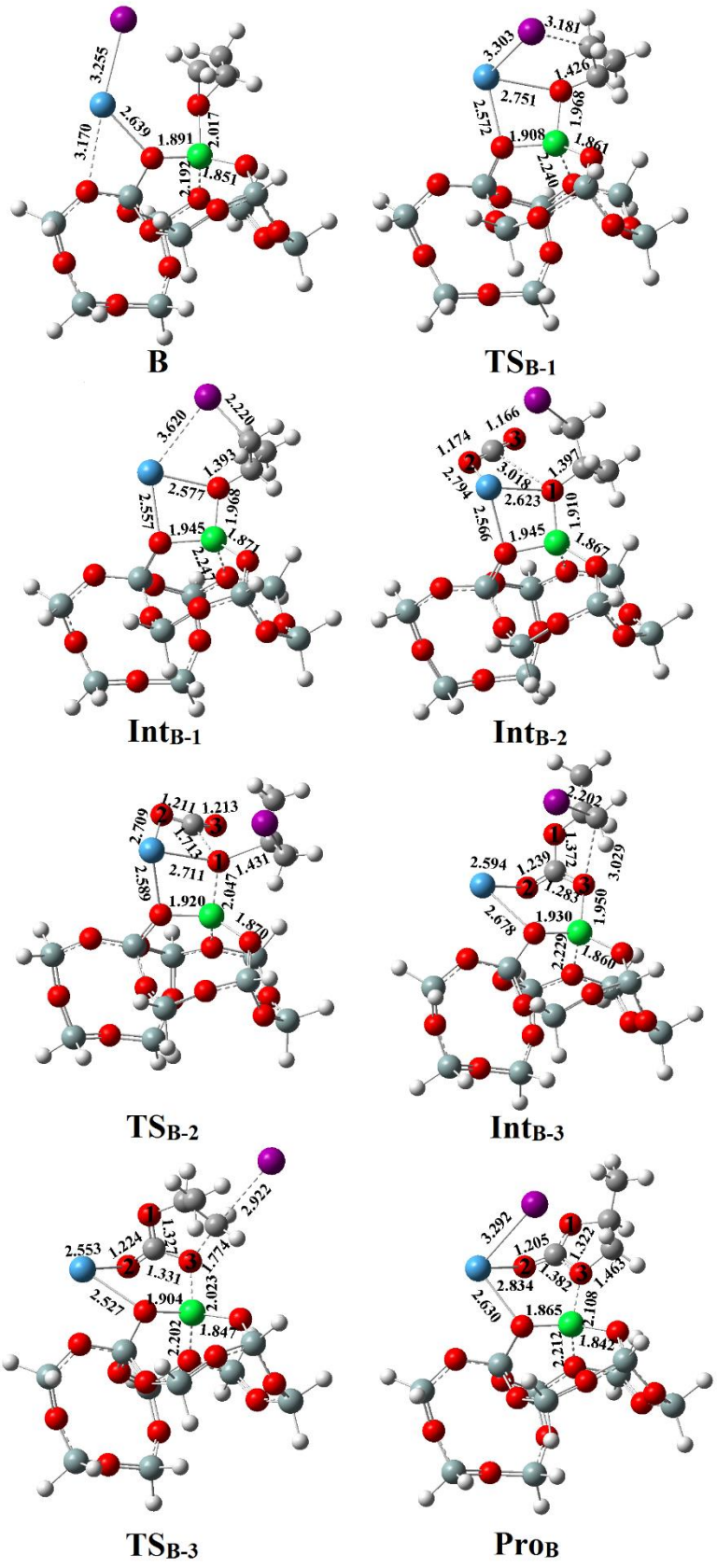

Fig. 6 The B3LYP/6-31G(d) optimized geometries of reactants, intermediates, transition states and products in Reaction B catalyzed by Zn-SBA-15/KI. Si – cyan, O – red, H – white, Zn – green, K

– blue, I – purple.

Reaction mechanisms were further considered by DFT model calculations. The B3LYP/6-31G(d)-optimized structures for SBA-15/KI (Reaction A) and Zn-SBA-15/KI (Reaction B) catalyzed reactions are shown in Fig. 5 and 6, respectively. The Cartesian coordinates with optimized geometries of stable points calculated at B3LYP/6-31G(d) level of theory are listed in the Supporting Information, and the potential energy profiles are shown in Fig. 7. In the initial process of Reaction A, PO is adsorbed on the SBA-15 in the form of hydrogen bond between the O of PO and the OH of SBA-15, and in TS_{A-1}, KI attacks the C-O bond of PO *via* standard S_N2 mechanism to promote the ring-opening process. In this process, I^- anion attacks the C(2) in the opposite of O. However, for Reaction B, the interaction comes from the complexation between the O of PO and the Zn of Zn-SBA-15. In $TS_{B-1,}$ the PO can open ring almost independently (the distance of C and O reaches 2.056 Å after the ring-opening) *via* S_N1 mechanism. The role of KI is primarily stabilizing the ring-opening intermediate. The energy barriers of this process are 27.0 (TS_{A-1}) and 23.2 (TS_{B-1}) kcal·mol^{-1} for the two reactions, which also means that Zn is beneficial to the ring-opening process. In the next step, CO_2 is coupling with the activated PO. In both processes (Int_{A-2} and Int_{B-2}), CO_2 is adsorbed on the O of ring-opened PO. In TS_{A-2} and TS_{B-2}, two reactions show almost the same structures and the similar energy barriers at 11.6 and 13.0 kcal·mol^{-1}. However, the intermediates (Int_{A-3} and Int_{B-3}) of this process are obviously different in the structures and energies. In Int_{A-3}, CO_2 is bound to the O of ring-opened PO with the longer bond length of C-O bond (1.485 Å). In Int_{B-3}, because of complexation role of Zn, the O atom of CO_2 is bound to Zn. As a result, a stable complex is formed with a hexatomic ring structure (formed by CO_2, K, O, Zn atoms). Compared to Reaction A, in which the energy of Int_{A-3} equals almost to the energy of TS_{A-2} (the difference in energy is only 0.03 kcal·mol^{-1}), the CO_2 coupling process of Reaction B is clearly promising as Int_{B-3} is protected by the energy barrier (11.4 kcal·mol^{-1}) against reverse decomposition into CO_2. The ring-closing is the last step of CO_2 cycloaddition reaction. In both processes (TS_{A-3} and TS_{B-3}), with the O

attacking to the iodide-bound C atom and the I^- anion closing to K^+ cation, the PC molecule is produced and the catalyst regenerates. The energy barriers of these processes are 17.3 (TS_{A-3}) and 27.3 (TS_{B-3}) kcal·mol^{-1}, respectively. In fact, the lower energy barrier of TS_{A-3} could be resulted from the unstable Int_{A-3}.

Our DFT calculations above show that CO_2 is not easily coupled to the ring-opened intermediate under the catalysis of SBA-15/KI, but zinc modified SBA-15 catalyst system can form a stable complex with CO_2 and enhance the cycloaddition reaction of CO_2 with PO. The NBO analysis[38] is thus performed to reveal the donor-acceptor interaction of this complex. Second-order perturbation energies (E_2) are used to describe the total energy lowering because of the effect of orbital interaction. In general, the bigger E_2 value is consistent with the more significant amount of charge transfer, and the intermolecular charge transfer results in the increase of binding energy. Comparing the values of E_2 between the reactants in the two reactions, the PO-adsorption differences can be found. For Reaction A, the E_2 value of lone pair (LP) electron of O atom of PO (O1) and empty sigma antibonding orbital (σ*) of O-H bond of SBA-15 (i.e., LP(O1) → σ*(O-H)) is 19.99 kcal·mol^{-1}. However, for Reaction B, The E_2 values of LP(O1) and three empty orbitals (LP*) of Zn (i.e., LP(O1) → LP*(Zn)) are 20.12, 17.62 and 11.24 kcal·mol^{-1}, respectively. It means a stronger donor-acceptor interaction of O1 with Zn than with hydroxyl owing to more empty orbitals of Zn (i.e., 4*s* and 4*p* orbitals). In addition, the sum of NBO charge for PO is 0.049 and 0.082 for Reaction A and B, respectively, i.e., the electron density of PO decreases more when bound to Zn, suggesting that the activation of Zn is slightly better than hydroxyl. The values of intramolecular E_2 are also compared between Int_{A-3} and Int_{B-3}. The intramolecular charge transfer towards the antibonding orbital (i.e. intramolecular LP → σ* interaction) is regard as the negative hyperconjugation to weaken the chemical bond. In Int_{A-3}, the E_2 values of LP(O2), LP(O3) and σ*(C-O1) (i.e., LP(O2) → σ*(C-O1) and LP(O3) → σ*(C-O1)) are 31.90 and 44.03 kcal·mol^{-1}, however, the E_2 values of LP(O1) → σ*(C-O3) is only 11.20 kcal·mol^{-1}. The results show that in Int_{A-3}, the C-O1 bond is weakened sharply, however, the C-O3 bond is only weakened slightly. As results, the interaction between C and O1 is weak; C-O3 bond is almost double bond

(1.221Å in Int_{A-3}) as in CO_2 molecule (1.169Å at the same level of theory). Considering the small energy difference (0.03 kcal·mol^{-1}) between Int_{A-3} and TS_{A-2} in Fig. 7, CO_2 molecule is regarded as adsorption on the O1 rather than coupling with PO in Int_{A-3}.

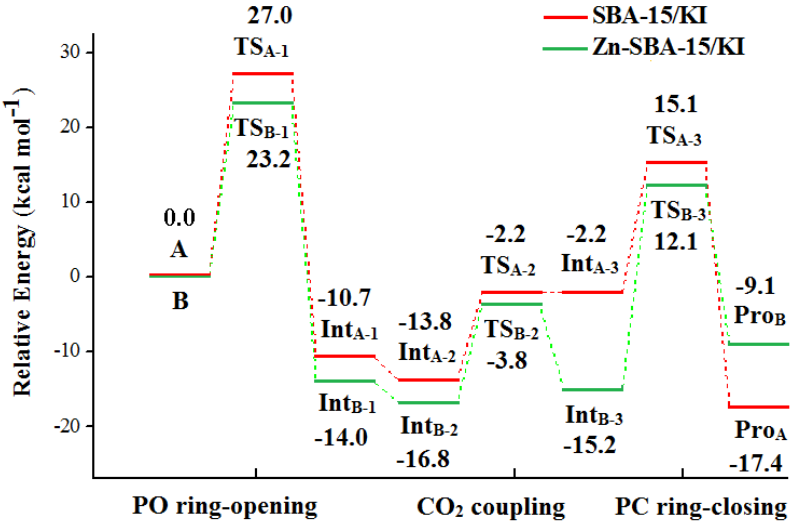

Fig. 7 Energy profile of minimum energy path (MEP) for SBA-15/KI- and Zn-SBA-15/KI-catalyzed cycloaddition reaction of PO with CO_2 calculated at the B3LYP/6-311++G(d,p)//B3LYP/6-31G(d) level of theory. ZPE at 6-31G(d) was taken into account.

From the proposed mechanism combined with minimum energy path derived from DFT calculation, we conclude that the major difference which can be found between zinc and without zinc modified catalysts is the coupling mode of CO_2 (Int_{B-3} *vs*. Int_{A-3}). The zinc species in Zn-SBA-15/KI can couple the O atom of CO_2 efficiently and form the stable intermediate to enhance the cycloaddition reaction, however, SBA-15/KI can only adsorb CO_2 physically. And Lewis acid Zn site exhibits stronger role than -OH towards epoxide activation. And after the loaded Zn species consumed all the silanol groups, one of the interesting aspects is the fact that the Zn-SBA-15/KI promoted reaction gives rise to S_N1 chemistry, brought about by the presence of both K and Zn in the transition state leading to the alkoxide intermediate. Bo et al.[39] also reported the detailed study on the formation of cyclic carbonate from PO/CO_2 over Zn(salphen)/NBu_4I binary catalytic system. By comparing our protocol with Bo et al., the epoxide ring-opening almost shows the similar energy barriers (23.2 *vs*. 22.4

kcal·mol^{-1}), the step that CO_2 reacts with the negatively charged oxygen atom (insertion) of the ring-opened intermediate is rate-determining with an energy value of 34.4 kcal·mol^{-1} over Zn(salphen)/NBu_4I catalysts, while using Zn-SBA-15/KI catalysts, the ring-closing reaction shows the rate-determining step with an lower energy value of 27.3 kcal·mol^{-1} based on our calculation results.

Experimental

Catalyst preparation and characterization

SBA-15 based samples modified with metal species (Zn, Fe, Ni, Co) were synthesized using nitrate salt precursors.[25,29,40] For the preparation of Zn-SBA-15, 2.0 g of triblock copolymer P123 (Sigma-Aldrich) was dissolved into 75.0 g of 1.6 M HCl (Sinopharm Chemical Reagent), a certain amount of zinc nitrate (Tianjin Kemiou Chemical Reagent) was added, and the mixture was stirred for 0.5 h. Thereafter, 4.0 g tetraethylsilicate (TEOS, Tianjin Kemiou) was added under stirring at 40 ºC. The resultant solution was stirred at 40 ºC for 24 h and then transferred into an autoclave; the mixture was subjected to heat treatment at 100 ºC for 24 h under static conditions. Finally, the liquid component was evaporated with stirring at 80 ºC, the solid material obtained was heated at 550 °C for 6 h with a heating rate of 1 ºC min^{-1} in air. The as-prepared metal modified SBA-15 samples were denoted as M(X)-SBA-15, where M and X represent the modified metallic element and the M/Si molar ratio in the material, respectively.

The M-SBA-15 samples prepared were characterized by different methods. FT-IR spectra were collected on a PerkinElmer Spectrum 100 FT-IR Spectrometer with a pelletized specimen diluted with anhydrous KBr (Tianjin Kemiou). X-ray diffraction (XRD) measurements were carried out using a Bruker D8 Advance X-ray powder diffractometer with Cu Kα radiation (40 kV, 40 mA) for phase identification. N_2 adsorption-desorption isotherms were collected at -196 °C using a Micromeritics ASAP 2000 system for samples degassed at 150 ºC for 12 h. For transmission electron microscopy (TEM), a sample was dispersed in ethanol and placed on a Cu grid. TEM measurements were conducted on Tecnai G2 Spirit with an operation voltage of 120 kV.

Metal content of the samples was determined by inductively coupled plasma optical emission spectrometer (ICP-OES) analysis using a PerkinElmer 8300 instrument.

Synthesis of cyclic carbonate from epoxides and CO_2

The reaction experiments were carried out in a 50 mL high pressure stainless-steel autoclave equipped with a magnetic stirring bar. In a typical run, the autoclave was firstly purged with CO_2 (99.99% purity, Harbin Qingha) to remove air and loaded with 0.10 g catalysts (0.05 g Zn-SBA-15 and 0.05 g KI). Then, 2.0 g (34.5 mmol) of PO (Aladdin Chemical Co.) was charged into the autoclave. The autoclave was heated to the required temperature (80 ºC in most cases) and CO_2 was introduced to a pressure of 1.0 MPa. After reaction, the autoclave was cooled to 0 ºC in an ice-water bath and depressurized slowly and carefully. The reaction mixture was centrifuged to recover the solid catalysts and the products were analyzed on GC (Agilent 7890A) equipped with a capillary column (Agilent 19091J-413) using flame ionization detector. In addition to PO, other epoxides were also tested, including 1,2-epoxybutane, epichlorohydrin, styrene oxide and cyclohexene oxide (Aladdin Chemical Co.). The catalyst recyclability was also examined for the coupling of CO_2 and PO. The catalyst samples (Zn-SBA-15, KI) were recovered and separated by centrifuge after the first run, dried at 60 ºC under vacuum, and then reused for the second run. The KI co-catalyst was partially soluble in the product of propylene carbonate, causing a slight loss in the weight of KI in the solid catalyst recovered. So, some amounts of fresh KI were added to control the total amount of the catalyst system at 0.10 g.

Computational details

SBA-15 and Zn-SBA-15 clusters are modeled on the basis of the previous literature,[41] as shown in Fig. 8(a) and (b), respectively. In Zn-SBA-15 model, the zinc replaces the two hydrogens of hydroxyl. DFT calculation was performed using GAMESS program.[42] B3LYP function was chosen to optimize the geometries and calculate the energies of the reactants, intermediates, transition states and products. The 6-31G(d) basis set was applied for hydrogen (H), carbon (C), oxygen (O), silicon (Si), potassium

(K) and zinc (Zn) atoms, and Lanl2dz basis set was used to describe iodine (I) atom. The corresponding harmonic vibration frequency calculations were also evaluated at the B3LYP/6-31G(d) level of theory to verify the local minima points of the potential energy surface with all the positive frequencies and saddle points with one imaginary frequency. The intrinsic reaction coordinate (IRC) method was used to construct the minimum energy path (MEP). Finally, the 6-311++G(d,p) basis set was performed to improve the reaction potential energies, and zero-point energy (ZPE) was also taken into account.

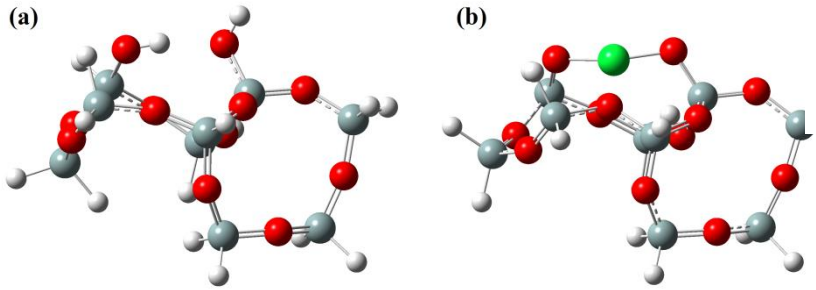

Fig. 8 B3LYP/6-31G(d) optimized geometries of (a) SBA-15 and (b) Zn-SBA-15. Si – cyan, O – red, H – white, Zn – green.

Conclusions

The selective production of cyclic carbonates via cycloaddition of CO_2 to epoxides can be achieved with a composite catalyst system of Zn-modified SBA-15 and KI under milder conditions (80ºC, 1 MPa, solvent-less) as compared to previous works in the literature (Table 4). The desired cyclic carbonates are obtained in a selectivity of 99% for several epoxides examined including propylene oxide, 1,2-butene oxide, (chloromethyl)ethylene oxide, (±)-phenylethylene oxide, and 1,2-cyclohexene oxide. The perfect catalytic performance appears at Zn/Si of 0.15 in mole and the amounts of Zn-SBA-15 and KI are the same in mass (or 1:3 molar ratio of zinc species to KI). The catalyst system may be recyclable with a small loss in the activity because a small amount of KI (20% of the initial amount of KI loaded) is not recovered during the catalyst separation and recovery. The feasible reaction mechanisms are proposed and

further considered by DFT model calculations. The zinc-modified catalyst not only undergoes electrostatic interaction with KI, but also binds the oxygen atom of epoxide to activate the epoxy ring. It shows different coupling modes of CO_2 and rate-determining step in the cycloaddition reaction compared with unmodified SBA-15/KI catalysts, which are promising results and have not been reported elsewhere.

Acknowledgements

We sincerely acknowledge the financial supports from National Natural Science Foundation of China (21373069), Science Foundation of Harbin City (NJ20140037), State Key Lab of Urban Water Resource and Environment of Harbin Institute of Technology (HIT2015DX08) and the Fundamental Research Funds for the Central Universities (HIT. IBRSEM. 201327).

Notes and references

1 (*a*) P. N. Pearson and M. R. Palmer, *Nature*, 2000, **406**, 695–699; (*b*) X. B. Lu and D. J. Darensbourg, *Chem. Soc. Rev*., 2012, **41**, 1462–1484.

2 (*a*) M. Cokoja, C. Bruckmeier, B. Rieger, W. A. Herrmann and F. E. Kühn, *Angew. Chem. Int. Ed.*, 2011, **50**, 8510–8537; (*b*) C. Martín, G. Fiorani and A. W. Kleij, *ACS Catal*., 2015, **5**, 1353–1370.

3 (*a*) B. M. Bhanage and M. Arai (Eds.), Transformation and Utilization of Carbon Dioxide, Springer-Verlag, Berlin, Heidelberg, 2014, p. 4–29; (*b*) M. Mikkelsen, M. Jørgensen and F. C. Krebs, *Energy Environ. Sci*., 2010, **3**, 43–81.

4 B. M. Bhanage, S. Fujita, Y. Ikushima and M. Arai, *Appl. Catal. A: Gen*., 2001, **219**, 259–266.

5 Y. Kayaki, M. Yamamoto and T. Ikariya, *Angew. Chem*., 2009, **121**, 4258–4261.

6 (*a*) C. J. Whiteoak, N. Kielland, V. Laserna, E. C. Escudero-Adán, E. Martin and A. W. Kleij, *J. Am. Chem. Soc*., 2013, **135**, 1228−1231; (*b*) M. North, S. C. Z. Quek, N. E. Pridmore, A. C. Whitwood and X. Wu, *ACS Catal*., 2015, **5**, 3398–3402; (*c*) S. Elmas, M. A. Subhani, M. Harrer, W. Leitner, J. Sundermeyer and T. E. Müller, *Catal. Sci. Technol*., 2014, **4**, 1652–1657.

7 (*a*) Y. Tsutsumi, K. Yamakawa, M. Yoshida, T. Ema and T. Sakai, *Org. Lett.*, 2010, **12**, 5728–5731; (*b*) S. S. Wu, X. W. Zhang, W. L. Dai, S. F. Yin, W. S. Li, Y. Q. Ren and C. T. Au, *Appl. Catal. A:*

Gen., 2008, **341**, 106–111.

8 (*a*) R. R. Kuruppathparambil, T. Jose, R. Babu, G. Y. Hwang, A. C. Kathalikkattil, D. W. Kim and D. W. Park, *Appl. Catal. B: Environ*., 2016, **182**, 562–569; (*b*) W. Y. Gao, Y. Chen, Y. H. Niu, K. Williams, L. Cash, P. J. Perez, L. Wojtas, J. F. Cai, Y. S. Chen and S. Q. Ma, *Angew. Chem. Int. Ed*., 2014, **53**, 2615–2619; (*c*) C. M. Miralda, E. E. Macias, M. Zhu, P. Ratnasamy and M. A. Carreon, *ACS Catal*., 2012, **2**, 180−183.

9 P. Ramidi, P. Munshi, Y. Gartia, S. Pulla, A. S. Biris, A. Paul and A. Ghosh, *Chem. Phys. Lett*., 2011, **512**, 273–277.

10 (*a*) B. H. Xu, J. Q. Wang, J. Sun, Y. Huang, J. P. Zhang, X. P. Zhang and S. J. Zhang, *Green Chem*., 2015, **17**, 108–122; (*b*) S. G. Esfahani, H. B. Song, E. Păunescu, F. D. Bobbink, H. Z. Liu, Z. F. Fei, G. Laurenczy, M. Bagherzadeh, N. Yan and P. J. Dyson, *Green Chem*., 2013, **15**, 1584–1589; (*c*) Z. Z Yang, Y. F. Zhao, G. P. Ji, H. Y. Zhang, B. Yu, X. Gao and Z. M. Liu, *Green Chem*., 2014, **16**, 3724–3728; (*d*) P. Agrigento, S. M. Al-Amsyar, B. Sorée, M. Taherimehr, M. Gruttadauria, C. Aprile and P. P. Pescarmona, *Catal. Sci. Technol*., 2014, **4**, 1598–1607; (*e*) M. S. Liu, L. Liang, X. Li, X. X. Gao and J. M. Sun, *Green Chem*. 2016, **18**, 2851–2863.

11 S. G. Liang, H. Z. Liu, T. Jiang, J. L. Song, G. Y. Yang and B. X. Han, *Chem. Commun*., 2011, **47**, 2131–2133.

12 Y. B. Sun, C. Y. Cao, S. L. Yang, P. P. Huang, C. R. Wang and W. G. Song, *Chem. Commun*., 2014, **50**, 10307–10310.

13 K. R. Roshan, A. C. Kathalikkattil, J. Tharun, D. W. Kim, Y. S. Won and D. W. Park, *Dalton Trans.*, 2014, **43**, 2023–2031.

14 Z. L. Wu, H. B. Xie, X. Yu and E. H. Liu, *ChemCatChem*, 2013, **5**, 1328–1333.

15 J. Qu, C. Y. Cao, Z. F. Dou, H. Liu, Y. Yu, P. Li and W. G. Song, *ChemSusChem*, 2012, **5**, 652–655.

16 J. A. Kozak, J. Wu, X. Su, F. Simeon, T. A. Hatton and T. F. Jamison, *J. Am. Chem. Soc*., 2013, **135**, 18497−18501.

17 (*a*) J. K. Lee, Y. J. Kim, Y. S. Choi, H. Lee, J. S. Lee, J. Hong, E. K. Jeong, H. S. Kim and M. Cheong, *Appl. Catal. B: Environ*., 2012, **111–112**, 621–627; (*b*) M. S. Liu, F. X. Wang, L. Shi, L. Liang and J. M. Sun, *RSC Adv*., 2015, **5**, 14277–14284; (*c*) R. J. Wei, X. H. Zhang, B. Y. Du, Z. Q. Fan and G. R. Qi, *J. Mol. Catal. A: Chem.*, 2013, **379**, 38–45.

18 A. I. Adeleye, D. Patel, D. Niyogi and B. Saha, *Ind. Eng. Chem. Res*., 2014, **53**, 18647–18657.

19 Z. J. Huang, F. B. Li, B. F Chen, T. Lu, Y. Yuan and G. Q. Yuan, *Appl. Catal. B: Environ*., 2013, **136–137**, 269–277.

20 J. N. Appaturi and F. Adam, *Appl. Catal. B: Environ*., 2013, **136–137**, 150–159.

21 Z. J. Huang, F. B. Li, B. F. Chen and G. Q. Yuan, *Catal. Sci. Technol*., 2016, **6**, 2942–2948.

22 Y. Xie, T. T. Wang, R. X. Yang, N. Y. Huang, K. Zou and W. Q. Deng, *ChemSusChem*, 2014, **7**, 2110–2114.

23 B. Tian, X. Liu, C. Yu, F. Gao, Q. Luo, S. Xie, B. Tu and D. Zhao, *Chem. Commun*., 2002, **11**, 1186–1187.

24 E. P. Mikheeva, S. V. Koscheev, S. P. Ruzankin, G. M. Zhidomirov, S. A. Leontiev, V. G. Devjatov and A. E. Cherkashin, *J. Electron. Spectrosc*., 1998, **94**, 59–71.

25 (*a*) D. Zhao, J. Feng, Q. Huo, N. Melosh, G. H. Fredrickson, B. F. Chmelka and G. D. Stucky, *Science*, 1998, **279**, 548–552; (*b*) Z. Y. Wu, Q. Jiang, Y. M. Wang, H. J. Wang, L. B. Sun, L.Y. Shi, J. H. Xu, Y. Wang, Y. Chun, J. H. Zhu, Chem. Mater., 2006, 18, 4600–4608.

26 F. Martínez, G. Calleja, J. A. Melero and R. Molina, *Appl. Catal. B: Environ*., 2005, **60**, 181–190.

27 A. Martínez, C. López, F. Márquez and I. Díaz, *J. Catal*., 2003, **220**, 486–499.

28 H. Wan, X. Li, S. Ji, B. Huang, K. Wang and C. Li, *J. Nat. Gas. Chem*., 2007, **16**, 139–147.

29 S. F. Zhong, L. Liang, M. S. Liu, B. Liu and J. M. Sun, *J. CO_2 Util.*, 2015, **9**, 58–65.

30 T. Ema, Y. Miyazaki, J. Shimonishi, C. Maeda and J. Hasegawa, *J. Am. Chem. Soc*., 2014, **136**, 15270−15279.

31 J. Song, Z. Zhang, B. Han, S. Hu, W. Li and Y. Xie, *Green Chem*., 2008, **10**, 1337–1341.

32 T. Lescouet, C. Chizallet and D. Farrusseng, *ChemCatChem.*, 2012, **4**, 1725–1728.

33 J. Xu, F. Wu, Q. Jiang and Y. X. Li, *Catal. Sci. Technol*., 2015, **5**, 447–454.

34 Q. Su, J. Sun, J. Q. Wang, Z. F. Yang, W. G. Cheng and S. J. Zhang, *Catal. Sci. Technol*., 2014, **4**, 1556–1562.

35 V. Guillerm, Ł. J. Weseliński, Y. Belmabkhout, A. J. Cairns, V. D. Elia, Ł. Wojtas, K. Adil and M. Eddaoudi, *Nat. Chem*., 2014, **6**, 673–680.

36 J. Ma, J. L. Liu, Z. F. Zhang and B. X. Han, *Green Chem*., 2012, **14**, 2410–2420.

37 (*a*) C. C. Rocha, T. Onfroy, J. Pilmé, A. D. Nowicki, A. Roucoux and F. Launay, *J. Catal*., 2016, **333**, 29–39; (*b*) B. Zou, L. Hao, L. Y. Fan, Z. M. Gao, S. L. Chen, H. Li and C. W. Hu, *J. Catal*.,

2015, **329**, 119–129; (*c*) A. Decortes, M. M. Belmonte, J. B. Buchholz and A. W. Kleij, *Chem. Commun.*, 2010, **46**, 4580–4582; (*d*) M. S. Liu, B. Liu, L. Shi, F. X. Wang, L. Liang and J. M. Sun, *RSC Adv.*, 2015, **5**, 960–966.

38 NBO 5.9. E. D. Glendening, J. K. Badenhoop, A. E. Reed, J. E. Carpenter, J. A. Bohmann, C. M. Morales, and F. Weinhold, Theoretical Chemistry Institute (University of Wisconsin, Madison, 2001).

39 F. C. Gómez, G. Salassa, A. W. Kleij and C. Bo, *Chem. Eur. J.*, 2013, **19**, 6289–6298.

40 Y. M. Wang, Z. Y. Wu, Y. L. Wei and J. H. Zhu, *Micropor. Mesopor. Mat.*, 2005, **84**, 127–136.

41 (*a*) Z. Wang, D. Wang, Z. Zhao, Y. Chen and L. Lan, *Comput. Theo. Chem*., 2011, **963**, 403–411; (*b*) J. Shen, J. M. Hill, R. M. Watwe, B. E. Spiewak and J. A. Dumesic, *J. Phys. Chem. B*, 1999, **103**, 3923–3934.

42 M. W. Schmidt, K. K. Baldridge, J. A. Boatz, S. T. Elbert, M. S. Gordon, J. H. Jensen, S. Koseki, N. Matsunaga, K. A. Nguyen, S. J. Su, T. L. Windus, M. Dupuis and J. A. Montgomery, *J. Comput. Chem*., 1993, **14**, 1347–1363.